Energy & Environmental Science

COMMUNICATION

View Article Online
View Journal | View Issue

Cite this: *Energy Environ. Sci.*, 2015, **8**, 3160

Received 21st August 2015,
Accepted 15th September 2015

DOI: 10.1039/c5ee02589c

www.rsc.org/ees

Multi-ring aromatic carbonyl compounds enabling high capacity and stable performance of sodium-organic batteries†

Heng-guo Wang,[ab] Shuang Yuan,[bc] Zhenjun Si[a] and Xin-bo Zhang*[b]

Herein we report that organic compounds comprising planar C_6 ring structures and carboxylate groups can function as an excellent anode material for sodium-organic batteries. Systematic comparisons of different electrode materials including the multi-ring aromatic compounds with or without carboxylate groups are carried out, the Na insertion mechanism is proposed, and the factors determining the capacity and potential plateaus are also elucidated by experimental and theoretical analyses.

Establishing efficient and low-cost energy storage systems (EES) is one of the most important issues and has already attracted extensive attention in our daily life. High-energy lithium-ion batteries (LIBs) are now actively being developed as a prime candidate for such EES applications;[1–7] however, their high cost, limited resources and uneven global distribution present unavoidable challenges to industry in the foreseeable future. As an alternative, sodium-ion batteries (SIBs) have recently drawn significant attention because, unlike lithium, sodium resources are practically low cost, inexhaustible and ubiquitous. Moreover, sodium shares similar physical and chemical properties with lithium in many aspects; thus opportunities for fast-advancing SIB research can be found in state-of-the-art LIB technologies.[8–22] Recently, building upon the success of LIBs, the overwhelming majority of host materials in SIBs have relied heavily on depletable metal or carbon-based inorganic compounds prepared from limited mineral resources. In comparison, there have been few investigations on organic electrode materials for SIBs.[23–30] Therefore, there is an urgent need to prepare future electrode materials, shifting from inorganic to organic materials that are more abundant, from a viewpoint of sustainability.

Organic-based electrode materials are considered to be a promising alternative due to their numerous advantages, including their non-reliance on rare materials, infinite availability from easily accessible natural sources and biomass, well-known redox stability, low safety risks compared to transition metal oxides, and "easier" control of the HOMO/LUMO energetics.[31–37] Most importantly, organic compounds have structural flexibility because of their less rigid structure compared to inorganic compounds,[38] which in turn provides higher mobility for the relatively larger ionic radius (102 pm) of the Na ion than that of the Li ion (76 pm).[24] Accordingly, organic compounds would be very suitable electrode materials for SIBs, particularly for overcoming the problem of poor kinetic properties.[24] Recently, a series of aromatic carbonyl derivatives or their sodium salts have been developed as promising organic electrode materials for SIBs.[23–26] We notice that these organic compounds comprise planar C_6 ring structures, which are the basic structural units of graphene or other carbon-based electrode materials, and carboxylate groups, which connect to the aromatic core to form stable enolates. This leads to very important questions of whether Na^+ ions could insert planar C_6 ring structures similar to graphene without carboxylate groups and what role carboxylate groups play in multi-ring aromatic carbonyl compounds. Therefore, a further understanding of the electrochemical reactions during sodiation/desodiation of these compounds from the perspective of molecular structure is imperative.

Herein, perylene 3,4,9,10-tetracarboxylic dianhydride (PTCDA) and its derivative tetrasodium perylene 3,4,9,10-tetracarboxylic dianhydride (NaPTCDA) (Fig. 1a), which both have multi-ring aromatic structures along with two types of carboxylate groups, were chosen as electrode materials to further define the relationship between planar C_6 ring structures and carboxylate groups. Also, comparisons of different electrode materials including the multi-ring aromatic compounds without carboxylate groups, such as perylene, pyrene and truxene (Fig. 1b), were carried out, and the factors determining the capacity and potential plateaus were also elucidated by experimental and theoretical analyses.

[a] *School of Materials Science and Engineering, Changchun University of Science and Technology, Changchun 130022, China*
[b] *State Key Laboratory of Rare Earth Resource Utilization, Changchun Institute of Applied Chemistry, Chinese Academy of Sciences, Changchun 130022, China. E-mail: xbzhang@ciac.ac.cn; Fax: +86-431-85262235; Tel: +86-431-85262235*
[c] *Key Laboratory of Automobile Materials, Ministry of Education, Department of Materials Science and Engineering, Jilin University, Changchun 130022, China*

† Electronic supplementary information (ESI) available. See DOI: 10.1039/c5ee02589c

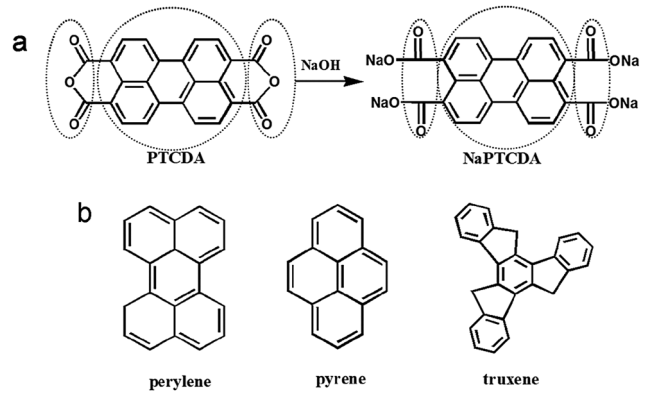

Fig. 1 Molecular structure of the multi-ring aromatic compounds tested as electrode materials.

All the molecules studied herein are either commercially available or easily synthesized by known and easy methods. PTCDA is a well-known organic semiconductor with good mechanical properties and high thermal stability; it is an especially low-cost chemical commodity largely prepared from acenaphthene, a coal tar component. Most importantly, it provides an ideal model to study the electrochemical reaction during sodiation/desodiation due to its low solubility. Further, its derivative, NaPTCDA, is successfully synthesized through a one-pot hydrolysis/sodiation reaction of the corresponding dianhydride (PTCDA) counterpart (Fig. 1a). First of all, we employ PTCDA as anode material for SIBs to investigate the sodium storage properties of multi-ring aromatic carbonyl compounds. Fig. 2a shows selected charge–discharge curves of the PTCDA electrode. The first charge–discharge cycle reveals the initial discharge and charge capacities to be 620.5 and 436.1 mA h g^{-1}, respectively, corresponding to a Coulombic efficiency of 60.9%. The large irreversible capacity loss likely originates from electrolyte decomposition, formation of the SEI layer at the lower potential range, and the irreversible bonding

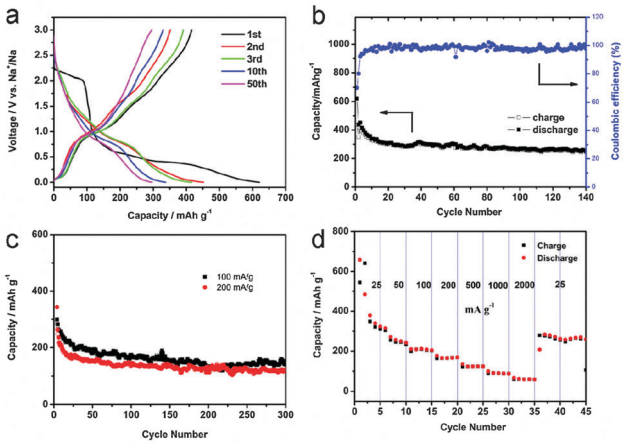

Fig. 2 (a) Charge–discharge curves and (b) cycle performance of PTCDA at a current density of 25 mA g^{-1}. (c) Cycle performance of PTCDA at current densities of 100 and 200 mA g^{-1}. (d) Rate performance of PTCDA at different current densities (25–2000 mA g^{-1}). All coin cells were cycled in the potential range of 0–3 V.

of Na^+ ions onto the condensed aromatic structures.[37] It is obvious that the low Coulombic efficiency is hard to avoid due to the low operating potentials; thus we should not blame the organic compounds.[30] Fortunately, its Coulombic efficiency increases dramatically upon cycling, reaching over 94% after 3 cycles and exceeding 98% after 10 cycles, suggesting that the insert and release of Na ions in each cycle are mostly equal. Moreover, the PTCDA electrode delivers a high second discharge capacity of 438.4 mA h g^{-1}. Considering the capacity contribution from acetylene black, it can still deliver a capacity of 361 mA h g^{-1} (Fig. S1, ESI†). The PTCDA electrode retains a reversible capacity of 250.5 mA h g^{-1} and a Coulombic efficiency of 100% after 140 cycles, corresponding to a capacity retention ratio of 40.4% (Fig. 2b). Unexpectedly, even at high current densities of 100 and 200 mA g^{-1}, the PTCDA electrode also delivers a reversible capacity of 144.6 and 117 mA h g^{-1} even after 300 cycles (Fig. 2c). Also, charge–discharge curves and cycle performance are recorded at a current density of 25 mA g^{-1} in the range 0.01–2 V (Fig. S2, ESI†). A reversible capacity of over 200 mA h g^{-1} and more than 30% capacity retention after 100 cycles could be obtained. To better understand the advantage of using multi-ring aromatic carbonyl compounds in SIBs, the rate performance of PTCDA is investigated (Fig. 2d). The electrode delivers initial reversible capacities of 315.4, 209.9, 176.4, 135.6, 99.8 and 67.7 mA h g^{-1} at current rates of 0.05, 0.1, 0.2, 0.5, 1 and 2 A g^{-1}, respectively. When the current density is reduced after the back-and-forth high rate and measurement after 35 cycles, a discharge capacity of 283.6 mA h g^{-1} can be recovered. Interestingly, at high temperature (55 °C), PTCDA can exhibit highly enhanced capacities of 719.9 and 659.3 mA h g^{-1} at the current densities of 25 and 100 mA g^{-1}, respectively (Fig. S3, ESI†). The presented results indicate that this organic compound shows superior electrochemical performance, including high reversible capacity, long cycling stability and good rate performance, which have surpassed those of the reported carbon-based anode materials ever measured for SIBs. Obviously, this organic compound is helpful for Na ion insertion, but the development of organic material for SIBs is still in the early stages. Electrolytes and binders also play an important role in enhancing the electrochemical properties.[18] In addition, surface modification of electrode materials is an effective way to improve electrochemical performance.[23]

To investigate the maximum amount of Na ions inserted into PTCDA, a smaller current density is applied. Fig. 3a shows the discharge curve at a current density of 10 mA g^{-1} in the potential range of 0–3 V. Obviously, the PTCDA electrode delivers an initial discharge capacity of 713 mA h g^{-1}, which is much higher than most SIB anodes, including hard carbon[14] and metal[20] or sulfides.[16] Our question is why and how the PTCDA electrode can deliver such high capacity. Theoretically, each formula unit of PTCDA transfers four electrons through the important enolization of the four carbonyl double bonds, which can deliver a theoretical specific capacity of 273 mA h g^{-1} (Fig. S4a, ESI†). Herein, the deep-discharge curve of PTCDA reveals that a two-stage discharge process could deliver the

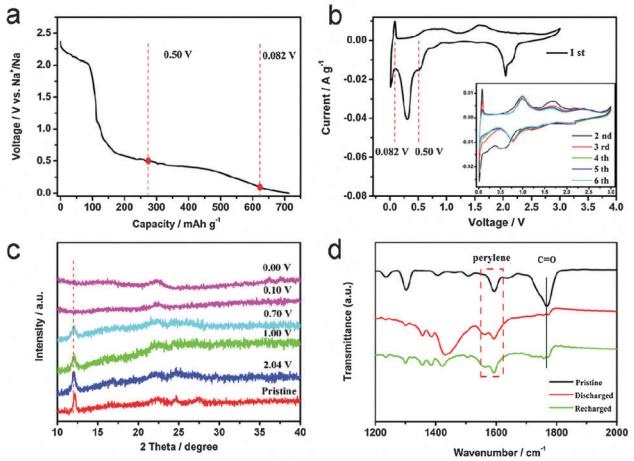

Fig. 3 (a) Discharge curves of PTCDA at a current density of 10 mA g^{-1} in the potential range of 0–3 V. (b) CV curves of PTCDA electrode between 0 and 3.0 V at a scan rate of 0.01 mV s^{-1}. (c) *Ex situ* XRD patterns of PTCDA before and after the first discharge process. (d) FTIR spectra of the pristine PTCDA, discharged to 0.0 V, and charged back to 3.0 V in the initial cycle.

theoretical specific capacity, where PTCDA captures four Na ions to form sodium enolate at the carbonyl group positions, as already discussed. Then, the following plateau at about 0.5 V and a long slope below 0.5 V eventually deliver a capacity of 440 mA h g^{-1}. Recent reports attributed this part of the capacity to the addition reaction between Li/Na ions and the unsaturated carbon.[39,40] If so, graphene composed of many unsaturated carbons may deliver super-high capacity, which will surpass the present results. In our opinion, this portion of the capacity should be attributed to the Na ion insertion in condensed aromatic structures and the formation of a solid electrolyte interphase (SEI) layer. In order to demonstrate this hypothesis, other multi-ring aromatic carbonyl compounds (NTCDA and PMDA) are also employed to investigate the sodium storage properties (Fig. S5, ESI†). It is obvious that the increase of benzene ring from PMDA to NTCDA and PTCDA has little impact on the capacity of these compounds. Therefore, this part of the capacity might not be attributed to the addition reaction between Li/Na ions and the unsaturated carbon. In addition, it is well known that formation of the SEI layer resulting from the irreversible reaction with the electrolyte could lead to the irreversible capacity, which is in accordance with Fig. 2a. The formation of the SEI layer is verified by XPS spectra[7] (Fig. S6 and S7, ESI†). Cyclic voltammetry (CV) is also conducted to investigate the electrochemical behaviors of the PTCDA electrode (Fig. 3b). The results are quite consistent with the charge–discharge profiles. Above 0.5 V, two pairs of well-resolved redox peaks appear, which are possibly associated with the formation of radical anion and then the dianion, respectively. In the cathodic scan, the sharp reduction peak at around 0.33 V, mainly during the first cycle and less pronounced in the following cycles, is characteristic of the electrolyte decomposition and formation of the SEI layer, consistent with Fig. 3a. Interestingly, the sharp peak in the first cathodic scan quickly diminishes in the second cycles, similar to LIB or SIB anode materials. In addition, a pair of redox peaks observed at a lower potential (near 0 V) is similar to lithium or sodium insertion in the interlayer of the carbonaceous materials.[6,17] Notably, the following CV curves almost overlap, indicating that the PTCDA electrode offers good stability.

To gain further insight into the Na ion insertion–deinsertion mechanism within PTCDA, *ex situ* XRD patterns and FTIR before and after the first discharge and charge processes are carried out. The XRD peaks at 12.4°, 24.8°, and 26.5° still remain after discharging to 0.7 V, suggesting that enolization of the four carbonyl double bonds does not destroy the crystal structure of PTCDA (Fig. 3c). However, after continuing to discharge (0 V) and charge (3 V), all XRD peaks vanish (Fig. S8, ESI†), which indicates that the insertion of Na ions to aromatic rings upon deep-discharge cycling turns the PTCDA structure completely amorphous. The loss of crystallinity is attributed to Na ion insertion in condensed aromatic structures[41] and/or to organic compound swelling by the electrolyte.[29] Obviously, following a deep discharge, the crystalline structure cannot be recovered. Our question is whether the change in molecular structure is also irreversible. Subsequently, we analyze the change in the bonding nature of PTCDA electrodes during battery operation using *ex situ* FTIR analysis. As shown in Fig. 3d, the absorbance signal at 1768 cm^{-1} attributed to the vibrational modes of the C═O double bonds in PTCDA is gradually weakened when discharging to 0 V, implying the reduction of the carbonyl groups. After recharging to 3.0 V, the intensity of this peak gradually recovers, indicating the participation of C═O double bonds in the reversible reaction with sodium. Moreover, the absorbance signals at 1593 cm^{-1} from the C═C stretching vibrations of perylene do not significantly change in the discharge and charge processes, indicating that no addition reaction between Na ions and the unsaturated carbon occurs. Therefore, there is no breakage of this bond upon Na-ion storage process, proof of the reversibility of the molecular structure.[29]

Subsequently, we employ the derivative (NaPTCDA) as anode material for SIBs to further investigate the sodium storage properties of multi-ring aromatic carbonyl compounds. Interestingly, modification from PTCDA to NaPTCDA results in the color change of the material from red to orange, which could be attributed to an energy gap enhancement between the respective HOMO and LUMO levels in the molecule resulting from the significant impact of the dianhydride opening on the inner electronic/bond structure of the perylene unit.[42] The complete opening of the dianhydride to form sodium carboxylate is revealed by FTIR spectra (Fig. 4a). One could notice that the intense band at 1768 cm^{-1} attributed to the vibrational modes of the C═O double bonds in PTCDA disappears, and the characteristic vibrations of salts of perylene tetracarboxylic acid at 1635 cm^{-1} and 1425 cm^{-1} (stretching vibration of –COO–) appear, which confirms the chemical structure of Na carboxylate groups conjugated with the perylene ring.[37,42] Then, we investigate the insertion of Na^+ ions in NaPTCDA. As shown in Fig. 4b, NaPTCDA delivered the initial discharge and charge capacities of 350.6 and 182.3 mA h g^{-1}, respectively. The 48% capacity loss can be mainly ascribed to the formation of the SEI, which is also verified by the sharp reduction peak (around 0.28 V) of the

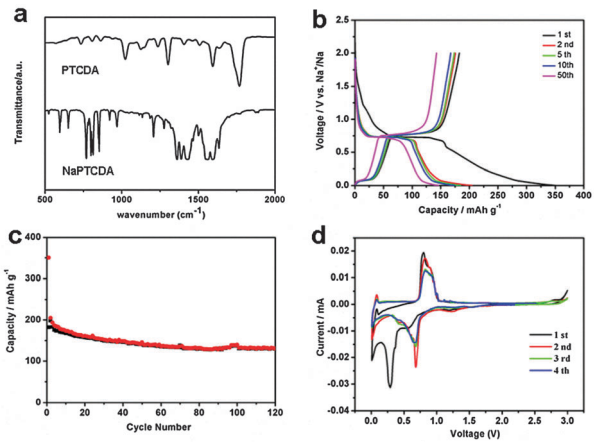

Fig. 4 (a) FTIR spectra of PTCDA and NaPTCDA, charge–discharge curves (b) and cycle performance (c) of NaPTCDA at a current density of 25 mA g^{-1}. (d) CV curves of NaPTCDA electrode between 0 and 3.0 V at a scan rate of 0.01 mV s^{-1}.

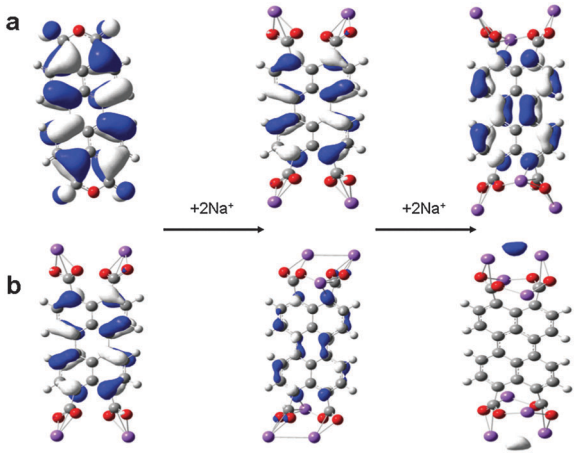

Fig. 5 HOMO plots of selected molecules/anions with different extents of reduction calculated at the B3LYP/6-31G(d) level: (a) PTCDA and (b) NaPTCDA.

CV curves (Fig. 4d). Theoretically, each formula unit of NaPTCDA also transfers four electrons through the important enolization of the four carbonyl double bonds, which can deliver a theoretical specific capacity of 206 mA h g^{-1}. In fact, the real capacity is derived from the two electrons transferred (Fig. S4b, ESI†), the formation of a SEI layer, and Na ion insertion in condensed aromatic structures. Moreover, the NaPTCDA electrode retains a reversible capacity of 131.1 mA h g^{-1} after 120 cycles, corresponding to a capacity retention ratio of 37.4% (Fig. 4c). Obviously, the low capacity further verifies that no capacity contribution from the addition reaction between Na^+ ions and the unsaturated carbon occurs. However, the capacity is comparable to the recently reported sodium terephthalate anode materials.[23–26] Interestingly, the different functional groups of PTCDA and NaPTCDA induce different electrochemical properties. The NaPTCDA electrode shows more distinctive discharge plateaus, low working voltage and narrow voltage gap, which are quite consistent with the CV curves (Fig. 4d). These results can be also explained from a theoretical view. According to molecular orbital theory, a lower LUMO energy means larger EA (electron affinity) and better oxidizability, and thus higher reduction potential.[32,36,43] To estimate the relative redox potential of these electrode materials, the HOMO/LUMO energy levels of related molecules are calculated by a DFT method. The results show that the LUMO (−3.97 eV) of PTCDA is lower than that of NaPTCDA (−1.49 eV). Therefore, the low discharge plateaus and narrow voltage gap of NaPTCDA are reasonable. Most importantly, both of them are ideal for the anode applications from the viewpoint of safety and energy density. In addition, a pair of obvious redox peaks are observed above 0.3 V, which is different from that of PTCDA, but similar to that reported for disodium terephthalate with two carbonyl groups, indicating that only two opposite carbonyl groups can combine with two Na^+ ions to form sodium enolate. In order to prove this hypothesis, the molecules bearing four carbonyls including PTCDA and NaPTCDA are subjected to DFT modeling (Fig. 5). When two Na^+ ions are captured at the opposite positions of carbonyl groups, the perylene ring can form an effective conjugated structure with carbonyl groups to help with stability; thus the HOMOs of Na_2–PTCDA and Na_2–NaPTCDA well localize within the structure. When it comes to four Na^+ ions, the HOMO of Na_4–PTCDA still well localizes within the structure, indicating the sufficient stability of PTCDA and explaining its successful four-Na uptake capability (Fig. S4a, ESI†). However, the HOMO of Na_4–NaPTCDA fails to retain within the structure, implying that the backbones of NaPTCDA are not able to support so much Na^+ ions and explaining its two-Na uptake capability (Fig. S4b, ESI†).[31]

Finally, we investigate the sodium storage properties of the compounds with the planar C_6 ring structures. As for the multi-ring aromatic structure core of PTCDA (the so-called perylene), if the electrochemical Na^+ ions could react with the unsaturated carbons to form Na/C complexes through addition reaction, it will deliver a large theoretical discharge capacity of 2125 mA h g^{-1}. In fact, the perylene electrode could only deliver a discharge capacity of 193 mA h g^{-1} even at the first cycle (Fig. S9a, ESI†). Similarly, two other compounds without carbonyl groups, pyrene and truxene, also delivered low discharge capacities of 205.9 and 199.1 mA h g^{-1}, respectively (Fig. S9b and S9c, ESI†). Obviously, these three compounds have different molecular structures and different numbers of benzene rings, but they deliver almost similar discharge capacity, indicating that no addition reaction between Na^+ ions and the unsaturated carbon occurs. The low capacity could be attributed to the formation of a SEI layer and Na ion insertion in condensed aromatic structures, even with the contribution from acetylene black.

The above results clearly demonstrate that organic compounds based on multi-ring aromatic carbonyl compounds show superior electrochemical performance for SIBs. Various evidences have verified no addition reaction occurring between Na^+ ions and the unsaturated carbon. However, the multi-ring can form a conjugated structure with carbonyl groups and promote the redox enolation reaction, thus playing an important role in the reversible Na^+ ion insertion/deinsertion. In addition, the presence of aromatic carbonyl groups not only captures Na^+

ions to form sodium enolate, but also plays a crucial role in the process of Na^+ ion insertion in condensed aromatic structures, thus enabling high capacity and stable performance. Certainly, efforts to further explore the Na^+ ion storage mechanism and tune the redox voltage through chemical modification of the molecular structure are currently in progress.

In summary, we have demonstrated that multi-ring aromatic carbonyl compounds enable sodium-organic batteries with high capacity and good performance. The high capacity (361 mA h g^{-1} at 25 mA g^{-1}), good rate performance (67.7 mA h g^{-1} at 2000 mA g^{-1}), and cycle life for 140 cycles are comparable to most SIB anodes, including hard carbon, alloys, and metal oxides or sulfides. Also, the electrochemical properties of Na^+ ion insertion in different organic compounds are compared. The results demonstrate that no addition reaction between Na^+ ions and the unsaturated carbon occurs, and the capacity and potential plateaus are tunable. Most importantly, sodium-organic batteries combine the attractive economics of sodium with the environmental benefits of organic materials, and they constitute an acceptable compromise among energy storage needs, reliability, cost, and pollution.

Acknowledgements

This work is financially supported by 100 Talents Programme of The Chinese Academy of Sciences, National Program on Key Basic Research Project of China (973 Program, Grant No. 2012CB215500 and 2014CB932300) and National Natural Science Foundation of China (Grant No. 21101147, 21203176 and 21404014).

Notes and references

1 J. M. Tarascon and M. Armand, *Nature*, 2001, **414**, 359.
2 S. Xin, L. Gu, N.-H. Zhao, Y.-X. Yin, L.-J. Zhou, Y.-G. Guo and L.-J. Wan, *J. Am. Chem. Soc.*, 2012, **134**, 18510.
3 C. F. Zhang, H. B. Wu, C. Z. Yuan, Z. P. Guo and X. W. Lou, *Angew. Chem., Int. Ed.*, 2012, **51**, 9592.
4 Z. W. Seh, W. Y. Li, J. J. Cha, G. Y. Zheng, Y. Yang, M. T. McDowell, P.-C. Hsu and Y. Cui, *Nat. Commun.*, 2013, **4**, 1331.
5 L. Qie, W.-M. Chen, Z.-H. Wang, Q.-G. Shao, X. Li, L.-X. Yuan, X.-L. Hu, W.-X. Zhang and Y.-H. Huang, *Adv. Mater.*, 2012, **24**, 2047.
6 K. Tang, R. J. White, X. K. Mu, M. M. Titirici, P. A. van Aken and J. Maier, *ChemSusChem*, 2012, **5**, 400.
7 Z.-S. Wu, L. L. Xue, W. C. Ren, F. Li, L. Wen and H.-M. Cheng, *Adv. Funct. Mater.*, 2012, **22**, 3290.
8 N. Yabuuchi, M. Kajiyama, J. Iwatate, H. Nishikawa, S. Hitomi, R. Okuyama, R. Usui, Y. Yamada and S. Komaba, *Nat. Mater.*, 2012, **11**, 512.
9 J. F. Qian, M. Zhou, Y. L. Cao, X. P. Ai and H. X. Yang, *Adv. Energy Mater.*, 2012, **2**, 410.
10 Y. L. Cao, L. F. Xiao, W. Wang, D. Choi, Z. M. Nie, J. G. Yu, L. V. Saraf, Z. G. Yang and J. Liu, *Adv. Mater.*, 2011, **23**, 3155.
11 Z. L. Jian, W. Z. Han, X. Lu, H. X. Yang, Y.-S. Hu, J. Zhou, Z. B. Zhou, J. Q. Li, W. Chen, D. F. Chen and L. Q. Chen, *Adv. Energy Mater.*, 2013, **3**, 156.
12 Y. Sun, L. Zhao, H. Pan, X. Lu, L. Gu, Y.-S. Hu, H. Li, M. Armand, Y. Ikuhara, L. Chen and X. Huang, *Nat. Commun.*, 2013, **4**, 1870.
13 Z. L. Jian, L. Zhao, H. L. Pan, Y.-S. Hu, H. Li, W. Chen and L. Q. Chen, *Electrochem. Commun.*, 2012, **14**, 86.
14 Y. Wen, K. He, Y. J. Zhu, F. D. Han, Y. H. Xu, I. Matsuda, Y. Ishii, J. Cumings and C. S. Wang, *Nat. Commun.*, 2014, **4**, 4033.
15 K. Tang, L. J. Fu, R. J. White, L. H. Yu, M.-M. Titirici, M. Antonietti and J. Maier, *Adv. Energy Mater.*, 2012, **2**, 873.
16 D. Y. W. Yu, P. V. Prikhodchenko, C. W. Mason, S. K. Batabyal, J. Gun, S. Sladkevich, A. G. Medvedev and O. Lev, *Nat. Commun.*, 2013, **4**, 2922.
17 H.-G. Wang, Z. Wu, F.-L. Meng, D.-L. Ma, X.-L. Huang, L.-M. Wang and X.-B. Zhang, *ChemSusChem*, 2013, **6**, 56.
18 S. Komaba, W. Murata, T. Ishikawa, N. Yabuuchi, T. Ozeki, T. Nakayam, A. Ogata, K. Gotoh and K. Fujiwara, *Adv. Funct. Mater.*, 2011, **21**, 3859.
19 H. Kim, R. A. Shakoor, C. Park, S. Y. Lim, J. S. Kim, Y. N. Jo, W. Cho, K. Miyasaka, R. Kahraman, Y. Jung and J. W. Choi, *Adv. Funct. Mater.*, 2013, **23**, 1147.
20 Y. H. Xu, Y. J. Zhu, Y. H. Liu and C. S. Wang, *Adv. Energy Mater.*, 2013, **3**, 128.
21 S. Yuan, X.-L. Huang, D.-L. Ma, H.-G. Wang, F.-Z. Meng and X. B. Zhang, *Adv. Mater.*, 2014, **26**, 2273.
22 S.-W. Kim, D.-H. Seo, X. H. Ma, G. Ceder and K. Kang, *Adv. Energy Mater.*, 2012, **2**, 710.
23 L. Zhao, J. M. Zhao, Y.-S. Hu, H. Li, Z. B. Zhou, M. Armand and L. Q. Chen, *Adv. Energy Mater.*, 2012, **2**, 962.
24 Y. Park, D. S. Shin, S. H. Woo, N. S. Choi, K. H. Shin, S. M. Oh, K. T. Lee and S. Y. Hong, *Adv. Mater.*, 2012, **24**, 3562.
25 A. Abouimrane, W. Weng, H. Eltayeb, Y. J. Cui, J. Niklas, O. Poluektov and K. Amine, *Energy Environ. Sci.*, 2012, **5**, 9632.
26 S. W. Wang, L. J. Wang, Z. Q. Zhu, Z. Hu, Q. Zhao and J. Chen, *Angew. Chem., Int. Ed.*, 2014, **53**, 5892.
27 K. Sakaushi, E. Hosono, G. Nickerl, T. Gemming, H. S. Zhou, S. Kaskel and J. Eckert, *Nat. Commun.*, 2013, **4**, 1485.
28 H.-G. Wang, S. Yuan, D.-L. Ma, X.-L. Huang, F.-L. Meng and X.-B. Zhang, *Adv. Energy Mater.*, 2014, **4**, 1301651.
29 E. Castillo-Martínez, J. Carretero-González and M. Armand, *Angew. Chem., Int. Ed.*, 2014, **53**, 5341.
30 W. Luo, M. Allen, V. Raju and X. L. Ji, *Adv. Energy Mater.*, 2014, **4**, 1400554.
31 Y. Liang, P. Zhang and J. Chen, *Chem. Sci.*, 2013, **4**, 1330.
32 Z. P. Song, Y. M. Qian, X. Z. Liu, T. Zhang, Y. B. Zhu, H. J. Yu, M. Otanibd and H. S. Zhou, *Energy Environ. Sci.*, 2014, **7**, 4077.
33 H. Y. Chen, M. Armand, G. Demailly, F. Dolhem, P. Poizot and J.-M. Tarascon, *ChemSusChem*, 2008, **1**, 348.
34 W. Guo, Y.-X. Yin, S. Xin, Y. G. Guo and L.-J. Wan, *Energy Environ. Sci.*, 2012, **5**, 5221.

35 X. Han, C. Chang, L. Yuan, T. Sun and J. Sun, *Adv. Mater.*, 2007, **19**, 1616.
36 Z. Song, H. Zhan and Y. Zhou, *Angew. Chem., Int. Ed.*, 2010, **49**, 8444.
37 R. R. Zhao, Y. L. Cao, X. P. Ai and H. X. Yang, *J. Electroanal. Chem.*, 2013, **688**, 93.
38 A. L. Goodwin, *Nat. Mater.*, 2010, **9**, 7.
39 X. Y. Han, G. Y. Qing, J. T. Sun and T. L. Sun, *Angew. Chem., Int. Ed.*, 2012, **51**, 5147.
40 J. S. Wu, X. H. Rui, C. Y. Wang, W.-B. Pei, R. Lau, Q. Y Yan and Q. C. Zhang, *Adv. Energy Mater.*, 2015, **5**, 1402189.
41 M. Hara, A. Satoh, N. Takami and T. Ohsaki, *J. Phys. Chem.*, 1995, **99**, 16338.
42 L. Fédèle, F. Sauvage and M. Becuwe, *J. Mater. Chem. A*, 2014, **2**, 18225.
43 M. Andrzejak, G. Mazur and P. Petelenz, *J. Mol. Struct.*, 2000, **527**, 91.